Glioblastoma ablates pericytes antitumor immune function through aberrant up-regulation of chaperone-mediated autophagy

Rut Valdor[a,b,1], David García-Bernal[a,2], Dolores Riquelme[a,b,2], Carlos M. Martinez[c], Jose M. Moraleda[a], Ana Maria Cuervo[d,e], Fernando Macian[f,e], and Salvador Martinez[g]

[a]Internal Medicine Department, Biomedical Research Institute of Murcia-Arrixaca, IMIB-Arrixaca, University of Murcia, 30120 Murcia, Spain; [b]Brain Regionalization and Development Gene Unit, Biomedical Research Institute of Murcia-Arrixaca, IMIB-Arrixaca, 30120 Murcia, Spain; [c]Experimental Pathology Unit, Biomedical Research Institute of Murcia-Arrixaca, IMIB-Arrixaca, 30120 Murcia, Spain; [d]Department of Developmental Molecular Biology, Albert Einstein College of Medicine, Bronx, NY 10461; [e]Institute for Aging Studies, Albert Einstein College of Medicine, Bronx, NY 10461; [f]Department of Pathology, Albert Einstein College of Medicine, Bronx, NY 10461; and [g]Instituto de Neurociencias, Consejo Superior de Investigaciones Científicas, University of Miguel Hernandez, Centro de Investigación Biomédica en Red de Salud Mental del Instituto de Salud Carlos III, 03550 San Juan de Alicante, Spain

Edited by Lawrence Steinman, Stanford University School of Medicine, Stanford, CA, and approved August 22, 2019 (received for review March 1, 2019)

The contractile perivascular cells, pericytes (PC), are hijacked by glioblastoma (GB) to facilitate tumor progression. PC's protumorigenic function requires direct interaction with tumor cells and contributes to the establishment of immunotolerance to tumor growth. Cancer cells up-regulate their own chaperone-mediated autophagy (CMA), a process that delivers selective cytosolic proteins to lysosomes for degradation, with pro-oncogenic effects. However, the possible impact that cancer cells may have on CMA of surrounding host cells has not been explored. We analyzed the contribution of CMA to the GB-induced changes in PC biology. We have found that CMA is markedly up-regulated in PC in response to the oxidative burst that follows PC–GB cell interaction. Genetic manipulations to block the GB-induced up-regulation of CMA in PC allows them to maintain their proinflammatory function and to support the induction of effective antitumor T cell responses required for GB clearance. GB-induced up-regulation of CMA activity in PC is essential for their effective interaction with GB cells that help tumor growth. We show that CMA inhibition in PC promotes GB cell death and the release of high immunogenic levels of granulocyte-macrophage colony stimulating factor (GM-CSF), through deregulation of the expression of cell-to-cell interaction proteins and protein secretion. A GB mouse model grafted in vivo with CMA-defective PC shows reduced GB proliferation and effective immune response compared to mice grafted with control PC. Our findings identify abnormal up-regulation of CMA as a mechanism by which GB cells elicit the immunosuppressive function of PC and stabilize GB–PC interactions necessary for tumor cell survival.

chaperone-mediated autophagy | pericytes | glioblastoma | tumor | immunosuppressive function

Glioblastoma multiforme (GB) is the most common and aggressive brain tumor. GB usually has a poor prognosis, with a median survival of 14 to 16 mo (1, 2). During its development, tumor cells infiltrate and invade the brain parenchyma, interacting with cells from perivascular areas and establishing a functional network of ultralong, microtube-like actin-rich membrane protrusions from GB (3–5). In recent years, several mechanisms have been reported to facilitate GB progression (6–10), including those requiring GB cell interactions with host cells for intercommunication and delivery of organelles and nutrients required to ensure tumor survival (3, 4, 11).

GB infiltrates the perivascular space and brain microvessels, which are composed of pericytes (PC) and endothelial cells (4, 11–13). PC are perivascular stromal cells that are situated on the abluminal vessel wall of brain capillaries. PC control multiple neurovascular functions and are required for neuronal homeostasis (14–16). PC regulate vessel tone and morphology, angiogenesis, and capillary hemodynamics (13–15). PC also contribute to the maintenance of the blood–brain barrier integrity through the elimination of toxic products, the control of the expression of endothelial tight junction and adherens proteins, and the regulation of vesicle trafficking (13–15, 17, 18).

PC may also develop stem cell-like properties, and release proregenerative growth factors and extracellular vesicles (18–20). PC are able to phagocytose and have the ability to promote inflammation in response to brain damage (16, 19), enhancing blood–brain barrier disruption through paracrine secretion of several vasculotoxic molecules and reactive oxygen species (ROS) (16, 18, 19). However, PC fail to contribute to the elimination of GB. The changes in PC biology that occur in response to the presence of GB tumor cells is not well understood yet.

We have recently shown that PC have an immunosuppressive function during GB progression, which contributes to the establishment of immune tolerance to the tumor and, therefore, to tumor growth (4). This switch in PC immune function is dependent on direct interactions between PC and tumor cells, which condition PC to develop an antiinflammatory phenotype responsible for the failure to activate T cell responses and the absence

Significance

Glioblastoma (GB) is the most lethal brain malignancy without an effective treatment. In this study, we demonstrate that tumor-induced change in chaperone-mediated autophagy (CMA) in host perivascular cells is a targetable process to prevent GB progression. CMA regulates pericyte interaction with tumor cells and sustains the acquired immunosuppressive function of pericytes, which is required for tumor survival. Blockage of CMA results in changes in the protein levels involved in cell-to-cell interaction and affects the pericyte secretory phenotype, resulting in defective GB adhesion and diminished tumor survival. This work reveals a previously unknown capacity of GB to modulate host pericyte CMA to assist in its own progression. Our results highlight the possibility of targeting CMA to treat this aggressive disease.

Author contributions: R.V. conceived and coordinated the study; R.V., A.M.C., F.M., and S.M. designed research; R.V., D.G.-B., D.R., and S.M. performed research; C.M.M., J.M.M., A.M.C., F.M., and S.M. contributed new reagents/analytic tools; R.V. analyzed and interpreted data; R.V. wrote the manuscript; and A.M.C. and F.M. provided advice and revised versions of the manuscript.

The authors declare no conflict of interest.

This article is a PNAS Direct Submission.

This open access article is distributed under Creative Commons Attribution-NonCommercial-NoDerivatives License 4.0 (CC BY-NC-ND).

[1]To whom correspondence may be addressed. Email: rut.valdor@um.es.

[2]D.G.-B. and D.R. contributed equally to this work.

This article contains supporting information online at www.pnas.org/lookup/suppl/doi:10.1073/pnas.1903542116/-/DCSupplemental.

First Published September 23, 2019.

Downloaded at Palestinian Territory, occupied on December 9, 2021

www.manaraa.com

of immune-mediated tumor clearance. Upon GB interaction, PC express high levels of the antiinflammatory cytokines IL-10 and TGF-β, and show decreased expression of the costimulatory molecules CD80 and CD86 and of histocompatibility complex molecules, MHC-II (4, 6, 7). Importantly, under those conditions, PC express the immunosuppressive PDL-1 ligand that can bind to programmed cell death 1 (PD-1) receptor expressed by T cells in the infiltrated GB perivascular areas (4, 7).

The molecular mechanisms underlying interactions between cancer cells and PC remain poorly characterized. Deciphering these mechanisms should lead to a better understanding of the host brain microenvironment during GB development and, most importantly, may allow finding novel therapeutic targets for effective GB treatment.

The GB-induced phenotypic switch of PC from pro- to antiinflammatory phenotype likely requires major changes of the PC proteome. Protein remodeling can be attained through changes in transcriptional programs as well as through active removal of proteins whose function needs to be terminated. Selective degradation of intracellular proteins occurs mainly via the ubiquitin proteasome system or by selective forms of autophagy. Chaperone-mediated autophagy (CMA) is a selective form of autophagy responsible for the targeted and timely degradation of soluble cytosolic proteins that have specific targeting motifs (biochemical related to the pentapeptide KEFRQ) in their amino acid sequence (21, 22). The cytosolic chaperone Hsc70 recognizes this motif and transports substrate proteins to the lysosomes (23). There, they are unfolded and transported into the lysosomal lumen for degradation through a translocation complex formed by multimers of the lysosomal receptor for CMA, LAMP-2A (24, 25). CMA activity is directly dependent on the levels of LAMP-2A at the lysosomal membrane, since the binding of substrate proteins to LAMP-2A is a limiting step for this pathway (22, 25). Lysosomal levels of LAMP-2A are usually regulated through changes in the turnover and intralysosomal distribution of this protein, and do not usually involve de novo protein synthesis (22). However, under conditions requiring maximal activation of this autophagic pathway, such as in response to oxidative stress, activation of CMA may occur through up-regulation of the expression of *Lamp2a* and synthesis of new proteins (26, 27). Regulation of the activity of CMA is critical to maintain cell function and homeostasis, as its failure leads to the intracellular accumulation of damaged proteins, defective regulation of many cellular processes, and altered responses to different stresses, such as nutrient deprivation, oxidative stress, or toxic exposure (25, 27, 28). CMA has been described as a regulatory mechanism of the function of some immune cells (26, 29); however, its role in PC is unknown. In this work, we have analyzed the contribution of CMA to the GB-induced PC phenotypic switch.

The immune function of PC may require tight regulation of levels of positive and negative regulators of signaling pathways that are induced by the interaction of these cells with GB (30–32). The ability of CMA to selectively degrade proteins in response to specific stimuli makes this mechanism an attractive candidate to contribute to the GB-induced functional switch in PC. We propose that CMA plays a role in the regulation of the ability of PC to modulate inflammation and, therefore, in the subsequent immune response in the perivascular niche to the presence of GB. Here, we present evidence that GB induces abnormal basal CMA up-regulation in PC, which is required to induce an immunosuppressive phenotype in PC that facilitates tumor progression. CMA also contributes to maintaining the stability of PC–GB interactions that GB needs to survive. Inhibition of CMA in PC promotes a secretory phenotype that contributes to the elimination of the tumor cells, and enhances changes in the immune properties of PC that prevent tumor progression.

Results

LAMP-2A Expression and CMA Activity Are Up-Regulated in PC in Response to the Oxidative Burst That Follows PC–GB Cell Interaction. PC acquire an immunosuppressive phenotype in response to direct GB interaction (GB-conditioned PC; ^{GBC}PC) (4). CMA can be utilized by different cell types to regulate their proteome through selective degradation of proteins and modulate their response to a wide variety of stimuli (22, 32). To determine if CMA contributed to the modulation of the functional switch that PC undergo during GB progression, we analyzed if LAMP-2A protein levels changed in PC following interaction with GB. Immunoblots of mouse LAMP-2A showed a marked increase of the levels of this protein in PC when grown in the presence of human GB (^{GBC}PC) (Fig. 1*A*). In addition, increased LAMP-2A protein levels correlated with an up-regulation of *Lamp2a* mRNA expression (Fig. 1*B*). Corroborating these data, an increase of luciferase activity, with similar kinetics to the induction of endogenous Lamp2a mRNA in ^{GBC}PC, was detected in PC transfected with a luciferase reporter vector controlled by the proximal promoter of the *Lamp2* gene (26) (*SI Appendix*, Fig. S1*A*).

In order to analyze if increased LAMP-2A protein levels in ^{GBC}PC required direct cell-to-cell interactions or was mediated by soluble molecules released by GB cells, we incubated PC for 48 h with sequential dilutions of supernatants obtained from GB cultures. Under these conditions, we did not find significant differences in *Lamp2a* expression when compared to the levels of *Lamp2a* mRNA in PC grown in control media (Fig. 1*C*). Immunofluorescence analyses using anti–LAMP-2A antibodies also evidenced increased LAMP-2A$^+$ puncta in ^{GBC}PC (Fig. 1*D*). However, flow cytometry analysis using the fluorescent lysosomal probe lysotracker did not show any difference in the total amounts of lysosomes in PC, whether conditioned or not by GB (Fig. 1*E* and *SI Appendix*, Fig. S1*B*), supporting the finding that the observed increase in LAMP-2A was not just a result of expansion of the lysosomal compartment but rather an increased level of LAMP-2A protein in lysosomes.

To determine if the increase in LAMP-2A protein levels resulted in higher CMA activity, we transfected PC with a vector that directs the expression of KFERQ-PA-mCherry-1, a photoactivable CMA reporter that allows monitoring CMA activity in living cells (33). Photoactivation of the KFERQ-PA-mCherry-1 reporter allows for detection of CMA activity by evaluating the numbers of mCherry$^+$ puncta, which result from the redistribution of the artificial fluorescent CMA substrate from the cytosol to the membrane of CMA-active lysosomes. Coculture of PC with GB cells significantly increased the number of mCherry$^+$ puncta per cell, supporting the finding that GB interaction induces CMA in PC (Fig. 1*F*). An inhibitor of macroautophagy, 3-methyladenine (3-MA), which has no effect on CMA, was used as control to confirm that mCherry cellular redistribution was not a consequence of activation of macroautophagy (Fig. 1*F*).

ROS release is known to regulate PC contractile properties in response to stressors to maintain blood vessel tone (18, 34); however, oxygen conditions in the perivascular invasive niche of GB have not been well defined (1). As mild oxidative stress activates CMA in several cell types through transcriptional up-regulation of *Lamp2a*, we analyzed if ROS production could be responsible for the increased *Lamp2a* expression in PC upon GB interaction. Surprisingly, whereas compared to basal levels no significant differences in ROS production were found in PC conditioned by culture with GB cells for 12 h (^{GBC}PC), GB cells produced higher levels of ROS in response to PC interaction (^{PCC}GB) compared to basal levels (Fig. 1*G*). To determine if this increase in ROS production by GB could contribute to the up-regulation of *Lamp2a* expression in PC, we treated cocultures of PC and GB with *N*-acetylcysteine (NAc), a ROS scavenger. In the presence of NAc, coculture with GB failed to induce an increase of the LAMP-2A protein levels in PC (Fig. 1*H*). In summary, our data support that the oxidative burst occurring in GB, caused by interaction with PC, could be responsible for the observed GB-mediated induction of CMA in PC.

GB-Induced CMA Activity in PC Is Required for the Acquisition of an Immunosuppressive Function in PC Following Interaction with GB. To determine if CMA activity was necessary for the establishment of the immunosuppressive function that PC acquire in response to interaction with GB (4), we isolated brain PC from WT control (WT PC) and LAMP-2A knockout (KO PC) mice (26) (Fig. 2*A*).

Downloaded at Palestinian Territory, occupied on December 9, 2021
www.manaraa.com

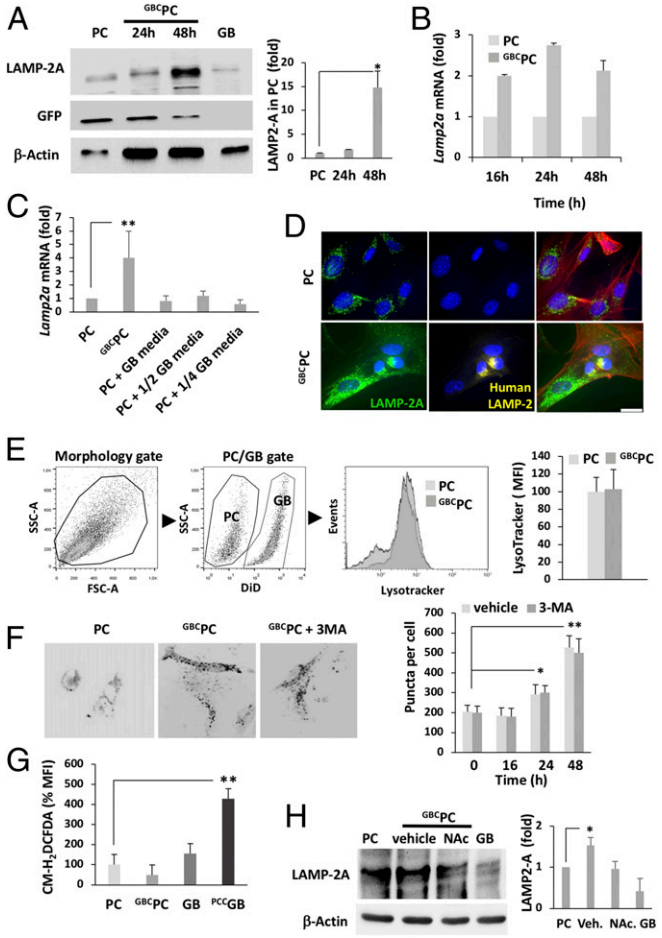

Fig. 1. GB interaction activates CMA in PC. (*A*) Immunoblot of LAMP-2A (representative of 5 experiments) in whole-cell lysates of GFP-expressing PC cocultured with GB (^{GBC}PC). LAMP-2A protein levels in human GB cells was used as negative control for murine LAMP-2A protein levels. Quantification by densitometry is represented as fold-induction of LAMP-2A levels (^{GBC}PC over PC) and normalized to GFP. $*P < 0.05$. (*B*) Quantification of *Lamp2a* mRNA expression by qPCR (relative to PC basal levels) in PC cocultured with GB cells (^{GBC}PC) (*C*) Semiquantitative analysis of *Lamp2a* mRNA expression by qPCR in PC, after being cultured for 72 h under several conditions (PC alone: PC; PC grown in presence of GB cells: ^{GBC}PC; PC grown in presence of several dilutions of GB conditioned media: PC + 1/2, 1/4 GB media); $**P < 0.01$. (*D*) LAMP-2A (green) identified by immunofluorescence in PC, under basal conditions and upon coculture with GB (^{GBC}PC) for 48 h. Nuclei were stained with DAPI (blue). GB cells were identified by human LAMP-2 protein (yellow). Phalloidin (red) was used to stain actin cytoskeleton. (Scale bar, 50 μm.). (*E*) Flow cytometry analysis of lysosome levels using lysotracker in control PC or ^{GBC}PC after 48 h. Gating strategy to identify DiD$^+$ GB-labeled cell population is shown (*Left*). Representative flow cytometry histogram and bar graph showing mean fluorescence intensity (MFI, normalized to values obtained from PC cultured alone). All data represent mean ± SD obtained from at least 4 independent experiments using U373 and U87 GB lines independently. (*F*) KFERQ-PA-mCherry distribution in PC transiently transfected with a CMA reporter vector, photoactivated and cocultured with GB cells in the presence or absence of 3-MA. Images show representative cells displaying mCherry$^+$ puncta (original magnification, 630×). Quantification is shown in bar graph (mean + SD of 3 different experiments with >50 cells counted per experiment) ($n = 3$; ANOVA with Tukey posttest; $*P < 0.05$; $**P < 0.01$). (*G*) ROS production measured by flow cytometry using CM-H2DCFDA in PC conditioned or not by GB cells (^{GBC}PC) and in GB cells conditioned or not by PC (^{PCC}GB) for 12 h. ROS production was not detected in initial hours of coculture. Data (mean + SD from 3 different experiments) are presented as MFI (normalized to values obtained from GB cultured alone); $**P < 0.01$. (*H*) Immunoblot of LAMP-2A in resting PC and PC conditioned by GB cells (^{GBC}PC) during 48 h in the presence or absence of NAc (representative of 3 different experiments). Quantification of the LAMP2-A levels is represented as fold-induction and normalized to levels of β-actin of both GB and PC. $*P < 0.05$.

Then, we analyzed the ability of WT and KO PC, previously conditioned or not by GB cells, to present ovalbumin $(OVA)_{323–329}$ peptide and activate OVA-peptide specific T cell receptor (TCR) transgenic OT-II CD4$^+$ T cells. As we had previously reported, the ability of WT PC to activate T cell responses was suppressed by the interaction with GB (4). However, in PC with impaired CMA activity (KO PC), interaction with GB failed to suppress the ability of PC to activate OT-II cells, and T cells maintained high levels of IL-2 production (Fig. 2*B*) and cell proliferation (Fig. 2*C*), even in the presence of GB cells. A reduced sensitivity of GB-mediated inhibition of PC's ability to activate T cells was also observed when *Lamp2a* expression was silenced in PC using short-hairpin RNA (shRNA) (*SI Appendix*, Fig. S1 *C* and *D*). Expression of the costimulatory molecule CD80 was markedly reduced in ^{GBC}WT PC compared to WT PC, but remained unaltered in ^{GBC}KO PC (Fig. 2*D*). Furthermore, the antiinflammatory phenotype that develops in ^{GBC}WT PC was also altered in CMA-deficient ^{GBC}KO PC, which showed reduced mRNA level expression of *Tgfb* and *Il10* (Fig. 2*E*) and higher levels of the proinflammatory cytokine TNF-α compared to ^{GBC}WT PC (Fig. 2*F*). In conclusion, these data suggest that functional CMA activity in PC is essential for the acquisition of the immunosuppressive function in response to GB interaction.

GB-Induced CMA in PC Is Required to Stabilize PC–GB Interactions That Maintain Tumor Cell Survival. GB may rely on their interactions with PC to support optimal proliferation and survival. We determined if persistence of these interactions required the observed CMA up-regulation in PC, and if, consequently, failure to activate this autophagic pathway could hinder GB tumor cell growth and survival. When we measured changes in cell proliferation of GB cells conditioned by WT or KO PC (Fig. 3*A*), we observed that GB proliferation was significantly reduced when grown in the presence of CMA-incompetent PC ($^{KO\ PCC}$GB) compared to control GB cells (GB) or GB cells cultured in presence of WT PC ($^{WT\ PCC}$GB) (Fig. 3*A*). Interestingly, we found that in GB–PC cocultures, GB cells showed abundant cell-to-cell interactions with WT PC, but they did not appear to interact properly with CMA-deficient KO PC (Fig. 3*B* and *SI Appendix*, Fig. S2*A*). Furthermore, a higher percentage of cell death was observed in $^{KO\ PCC}$GB cells compared to control GB cells or $^{WT\ PCC}$GB (Fig. 3*C*). Survival of PC was, however, not significantly affected by the presence of GB or the absence of CMA (Fig. 3*D*). Interestingly, similar to what happened in the presence of KO PC, we found high levels of cell death in GB cells cocultured with NAc-treated WT PC (*SI Appendix*, Fig. S2*B*).

We then proceeded to characterize in more detail the interactions between GB and PC using surface scanning electron microscopy. We noticed that, as previously described (3), GB cells interacted with PC through microtube-like ultralong protrusions (*SI Appendix*, Fig. S2*A*), and that PC projected small nanotubes toward the surface of the GB to sustain interaction (Fig. 3*E*). However, we hardly found those structures in KO PC. Instead, we observed disorganized protrusions in contact areas of KO PC with GB (Fig. 3 *E* and *F* and *SI Appendix*, Fig. S2*A*). To confirm these altered interactions, we also evaluated adhesion of GB to PC by measuring RFP fluorescence retained on a PC monolayer after washing away RFP$^+$ GB cells that had been cocultured with the PC monolayer for 24 h. We detected a significant loss of adherence (~35%) in GB cocultured with KO PC (Fig. 3*G*).

Furthermore, scanning microscopy analyses of GB cultured in the presence of WT or KO PC also revealed a different pattern of distribution of secretory vesicles in PC. While secretory vesicles often accumulated in the sites of contact between WT PC and GB, they were rarely observed in KO PC (*SI Appendix*, Fig. S2*C*). Morphometrics analyses of extracellular vesicles positive for CD63, a common marker of intracellular vesicle membranes, revealed that WT PC increased vesicle secretion in response to GB (*SI Appendix*, Fig. S3 *A* and *B*). Interestingly, although extracellular vesicle number in KO PC was higher than in WT PC, vesicle abundance remained unaltered when cultured in the presence of GB. Interestingly, only vesicles from ^{GBC}KO PC cultures were capable of inhibiting GB

Downloaded at Palestinian Territory, occupied on December 9, 2021
www.manaraa.com

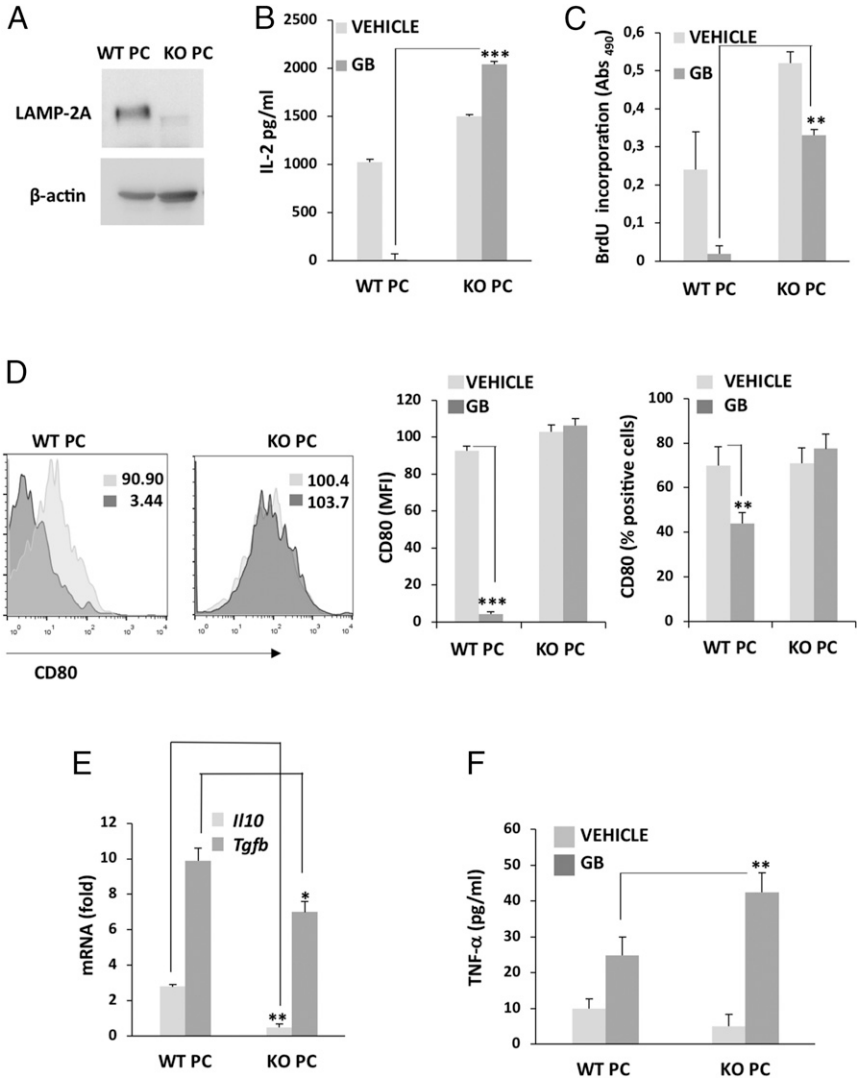

Fig. 2. GB-induced CMA activity in PC is required for the acquisition of an immunosuppressive function in PC following interaction with GB. (*A*) Immunoblot of LAMP-2A in PC of LAMP-2A KO (KO PC) or WT mice (WT PC). (*B*) IL-2 production was measured by ELISA after 72 h of stimulation of naïve OT-II $CD4^+$ T cells in response to $OVA_{323–339}$ peptide presented by KO PC conditioned (GB) or not (vehicle) by GB and compared to control WT PC. Values are normalized to basal levels of IL-2 in resting T cells. Results are mean + SD from 5 to 6 different experiments; $***P < 0.001$. (*C*) T cell proliferation was measured by BrdU incorporation in response to antigen presentation by WT PC and KO PC previously conditioned (GB) or not (vehicle) by GB. Results are mean + SD from 4 different experiments, $**P < 0.01$. (*D*) Flow cytometry analysis of the expression of the costimulatory molecule CD80. Insert numbers inside histograms represent MFI values. Bar graphs show MFI values and percentages of cells expressing CD80. Nonspecific fluorescence was measured using specific isotype monoclonal antibody and GB cells were used as negative control. Data represents mean ± SD obtained from at least 3 independent experiments, $**P < 0.01$; $***P < 0.001$. (*E*) mRNA expression of *Il10* and *Tgfb* assessed by qPCR in GB-conditioned WT PC and KO PC relative to basal levels in cells cultured in the absence of GB. Data (mean + SD from 3 different experiments) are presented as fold-induction of mRNA expression following coculture with GB for 72 h. $*P < 0.05$, $**P < 0.01$. (*F*) ELISA measuring TNF-α secreted by WT PC and KO PC cocultured with (GB) or without (vehicle) GB cells for 72 h. GB cells were used as negative control. All data represent mean ± SD obtained from at least 3 independent experiments; $**P < 0.01$.

proliferation (*SI Appendix*, Fig. S3*C*), suggesting that changes in CMA result in qualitative differences in vesicle composition/content rather than just mere changes in their abundance.

Coculture of GB with CMA-Deficient PC Results in the Secretion of Proteins That Reduce Tumor Cell Survival and Prevent PC–GB Interactions. To characterize the basis for the increased GB cell death in the absence of stable PC interactions, we analyzed differences in danger signals that could be released by GB (1, 8, 35) when cultured in presence of WT or CMA-deficient KO PC. Levels of granulocyte-macrophage colony stimulating factor (GM-CSF) produced by GB almost doubled when cocultured with WT PC, but secretion of this cytokine was much higher in the presence of KO PC (Fig. 4*A*). This increase in GM-CSF secretion by GB could be recapitulated by using conditioned media obtained from cocultures of KO PC and GB, but not of WT PC and GB (Fig. 4*B*). Furthermore, very high levels of ROS were detected in $^{KO\ PCC}$GB at 24 to 72 h of coculture (Fig. 4*C*), when GB cell death was occurring (Fig. 3*C*). Once again, changes in GB ROS production could be reproduced, even in presence of WT PC ($^{WT\ PCC}$GB), by using culture media from cocultures of KO PC and GB (Fig. 4*D*), suggesting that CMA-incompetent PC exposed to GB may secrete toxic molecules that negatively impact tumor survival.

We then proceeded to determine if that toxic secreted molecule would also affect the interactions between PC and GB. Indeed, we found that media obtained from GB-KO PC cocultures was also sufficient to reduce GB adhesion to WT PC (Fig. 4*E*), mimicking what we had seen in cocultures of GB and KO PC. This effect occurred if cells were treated with conditioned media either before or after GB–PC cell interactions had been formed, supporting that secreted molecules not only inhibited formation of GB–PC interactions but also disrupted pre-established ones. Furthermore, we observed that the media from $^{KO\ PCC}$GB was also sufficient to induce GB cell death, not only when cultured alone but also when GB was grown in the presence of WT PC (Fig. 5 *A* and *B*). To investigate the nature of the molecules that might be secreted by ^{GBC}KO PC, we subjected the conditioned media to treatment with proteases or ribonucleases. Treatment of conditioned media from ^{GBC}KO PC cultures with trypsin failed to induce GB cell death, whereas treatment with RNase did not alter the ability of the conditioned media to induce GB cell death. These findings support that secreted proteins or peptides are responsible for the toxic effect of the conditioned media on GB (Fig. 5*C*). We propose that these cytotoxic products may be part of the normal proinflammatory response of PC to the presence of GB, and that GB prevents their production/secretion by up-regulating CMA in PC cells.

GB-Induced CMA in PC Alters the Expression of Markers/Properties Associated with Mesenchymal Stem Cells and Contributes to Regulating Interactions with GB Cells. We next further investigated the role of CMA in the switch in PC function induced by GB, by

Downloaded at Palestinian Territory, occupied on December 9, 2021
www.manaraa.com

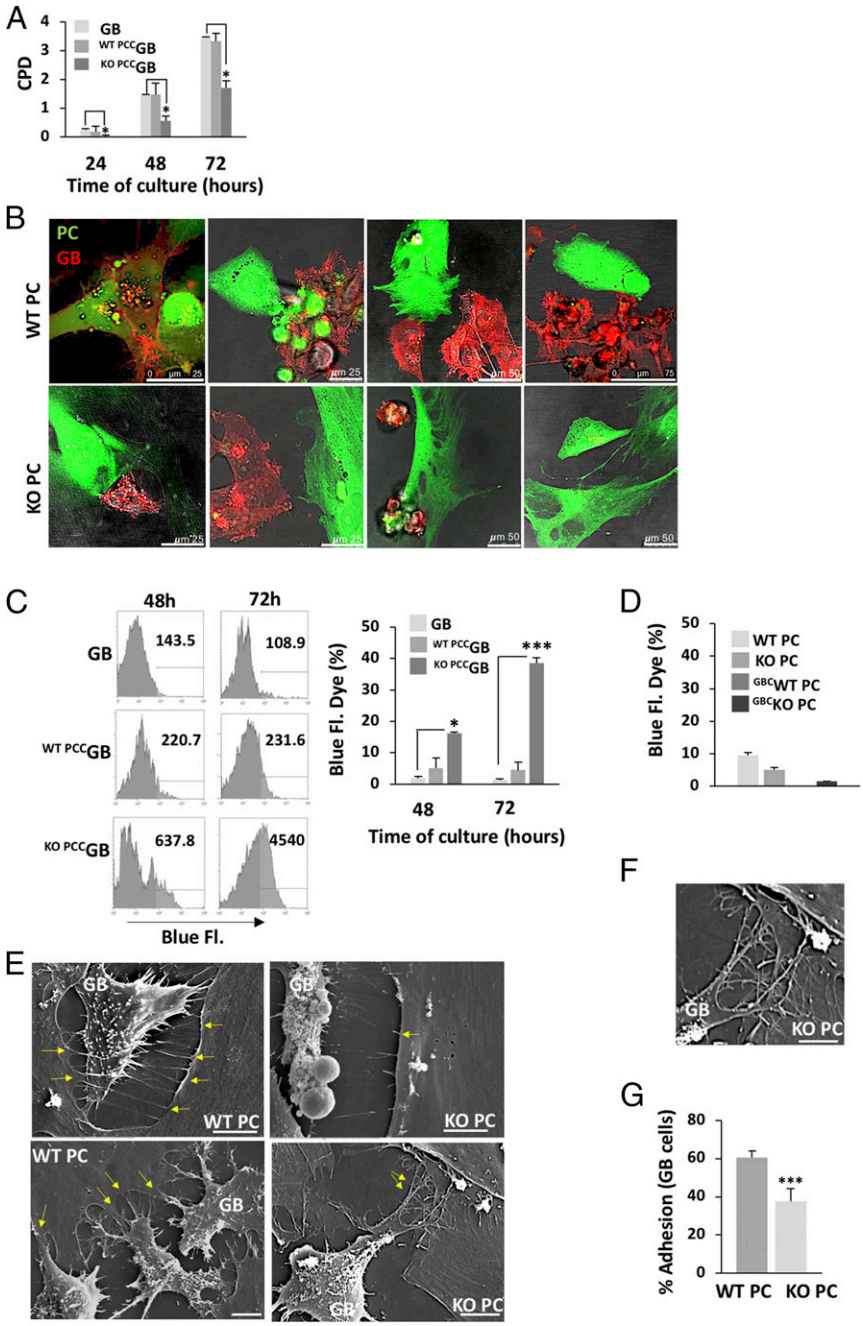

Fig. 3. GB-induced CMA in PC is required to stabilize PC–GB interactions. (*A*) Proliferation of GB cells interacting with WT PC ($^{WT\ PCC}$GB) or KO PC ($^{KO\ PCC}$GB), represented as cumulative population doubling (CPD), during different times of coculture was measured and compared to proliferation of control GB cells. Results are mean + SD of at least 3 different experiments; $*P < 0.05$. (*B*) Cell interactions between GB and WT PC or KO PC cocultured during 72 h, detected by confocal fluorescence microscopy. PC were previously stained with CFSE (green) and GB cells express the RFP-protein (red). Representative images are the merge of RFP and CFSE fluorescence with the phase contrast image. (Scale bars: 25, 50, and 75 μm.) (*C*) Detection of GB cell death by LIVE/DEAD blue-fluorescent reactive dye (blue-fluorescent dye), following coculture with WT PC or KO PC for 48 and 72 h. MFI is shown in representative histograms and graph bar represents quantification of dead cell percentages from at least 4 independent experiments, $*P < 0.05$ or $***P < 0.001$. (*D*) Detection of dead cells by blue-fluorescent reactive dye of WT PC or KO PC in presence or not of GB cells (^{GBC}WT PC; ^{GBC}KO PC) after 72 h of coculture. (*E*) Interaction of WT PC and KO PC with GB cells. Images obtained by scanning electron microscopy are representative of at least 3 independent experiments. Arrows indicate interaction through nanotubes (*Upper*) and cytosol fusion (*Lower*) after 72 h of coculture. (Scale bar, 10 μm.) (*F*) Magnified detail of disorganized protrusions in contact areas of KO PC. (Scale bar, 5 μm.) (*G*) Adhesion assay of GB cells expressing RFP with WT PC or KO PC cocultured for 24 h. Graph represents percentage of adhesion relative to fluorescent levels obtained in control cultures with GB cells alone of at least 3 independent experiments; $***P < 0.001$.

analyzing changes in phenotype that may result from exposing CMA-competent and CMA-defective PC to GB. We found in PC that several markers associated with mesenchymal stem cells (MSC) (14, 18, 20) were affected by the absence of CMA. As expected, WT PC proliferation was inhibited by GB; however, KO PC maintained their proliferative capacity in the presence of GB (Fig. 6*A*). Levels of the angiogenic cytokine IL-6 produced by PC, which is associated to altered PC proliferation and regenerative properties (4, 18–20), were clearly up-regulated by the presence of GB in WT PC. However, IL-6 expression remained unaffected when KO PC were analyzed in the same conditions (Fig. 6*B*). Levels of other angiogenic factors, such as vascular endothelial growth factor (VEGF) and angiotensin I (18, 20) were also increased in WT PC when cocultured with GB, whereas KO PC production of those factors was not affected by GB. On the other hand, the production of the antiangiogenic factor antithrombin (36, 37) was highly induced in KO PC but not in WT PC, when conditioned by the presence of GB (*SI Appendix*, Fig. S4 *A–C*). In addition, the osteogenic factor, osteonectin (Sparc), which has been reported to be associated to angiogenic inhibition and tumor growth (38, 39), was also up-regulated in KO PC in presence of GB (*SI Appendix*, Fig. S4*D*). Interestingly, when instead of the media we directly analyzed the secreted vesicular fraction, we also identified increased levels of osteonectin and IL-6 in the vesicles secreted by KO PC in presence of GB (*SI Appendix*, Fig. S4 *E* and *H*). Although low amounts of VEGF and antithrombin were also detected in vesicles from both WT PC and KO, the levels of VEGF were only increased by GB in WT PC (*SI Appendix*, Fig. S4 *E–G*).

Other changes induced by GB in WT PC, including a reduction in mitochondrial mass (*SI Appendix*, Fig. S5*A*) and changes in the expression of associated mesenchymal markers Sca-1, CD105, and CD90, did not occur in KO PC cocultured with GB (Fig. 6 *C–E*).

Downloaded at Palestinian Territory, occupied on December 9, 2021
www.manaraa.com

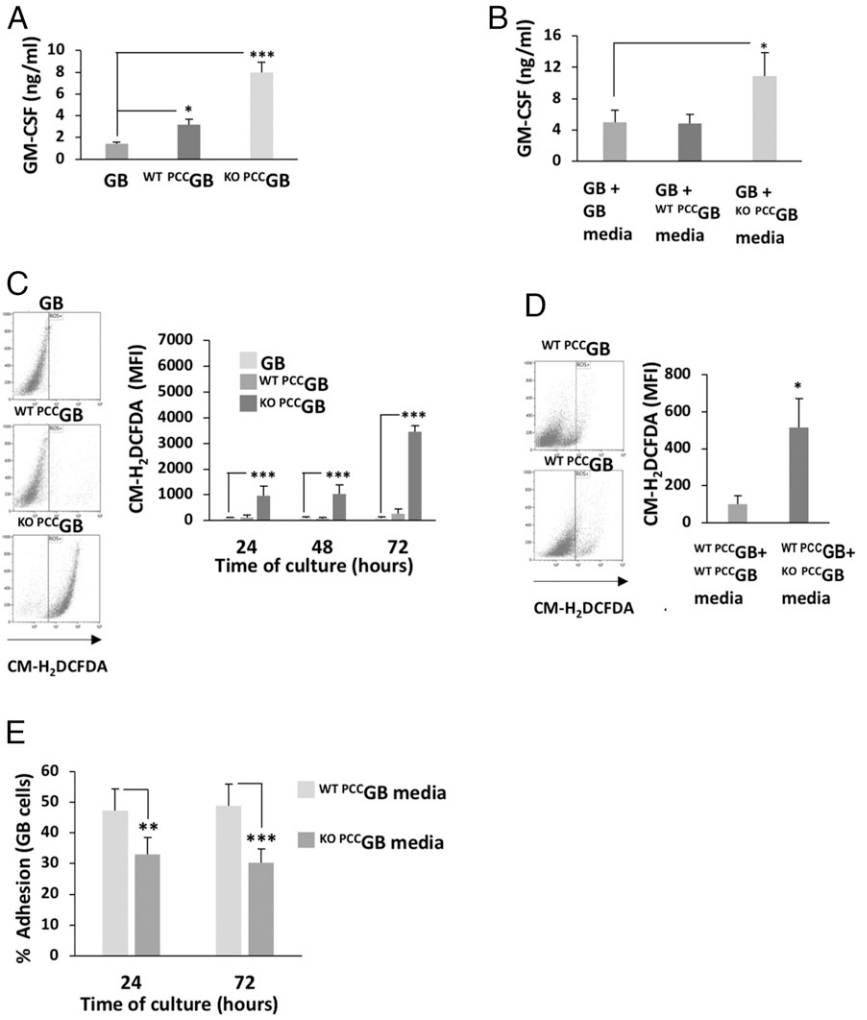

Fig. 4. GB-induced CMA in PC prevents tumor cell death. (*A*) ELISA measuring human GM-CSF levels produced by GB cells at basal levels and conditioned by WT PC ($^{WT\ PCC}$GB) or KO PC ($^{KO\ PCC}$GB) during 72 h. $*P < 0.05$, $***P < 0.001$. (*B*) ELISA measuring human GM-CSF levels produced by GB cells at basal levels and in presence of media obtained from cell cultures of WT PC and GB or KO PCC and GB cocultured for 72 h. All data represent mean ± SD from at least 3 independent experiments, $*P < 0.05$. (*C*) Flow cytometry analysis of ROS production in GB cells conditioned by WT PC ($^{WT\ PCC}$GB) or KO PC ($^{KO\ PCC}$GB) for 24 and 72 h. ROS production in PC was not detectable. Dot plots are representative experiments showing ROS production at 72 h. Graph bar represents MFI values normalized to values obtained from GB cultured alone of at least 3 independent experiments, $***P < 0.001$. (*D*) Flow cytometry analysis of ROS production in GB cells cultured with WT PC in the presence or absence of conditioned media from 72-h cocultures of GB and WT PC or GB and KO PC (ROS was not detectable in PC). Data represent mean ± SD (MFI normalized to values from control GB). of at least 3 independent experiments; $*P < 0.05$. (*E*) Adhesion assay of GB cells expressing RFP to a WT PC monolayer in presence of conditioned media from cultures of GB and WT PC or GB and KO PC. Equal values of adhesion were measured after 24 and 72 h. Graph represents percentage of adhesion relative to fluorescent levels of control GB cells alone of at least 4 independent experiments; $**P < 0.01$, $***P < 0.001$.

We also found that the expression of the interaction protein occludin, which was reduced in WT PC conditioned by GB cells, appear to be deregulated in KO PC, which showed high levels of expression (Fig. 6*F* and *SI Appendix*, Fig. S5*B*). All of these data together support that the induction of CMA caused by GB in PC, in addition to down-regulating the immune function of PC, is also essential to maintain the effective interaction of PC with GB cells and to regulate markers/properties associated with MSC in PC that may contribute to sustain tumor growth (Fig. 6*G*).

GB-Induced CMA in PC Assists Tumor Growth. We have seen previously that, when interacting with GB, PC fail to induce T cell responses in vitro, and facilitate GB proliferation and tumor growth in vivo (4). To determine if the induction of CMA caused by GB in PC might contribute in vivo to the regulation of those functions that assist tumor growth, we first analyzed if $CD4^+$ T cell responses would also be affected by the lack of CMA in PC in our GB mouse model (4). Purified $CD4^+$ T cells from lymph nodes of mice xenografted with WT PC and RFP^+ GB cells revealed significant decreased activation compared to cells isolated from control mice. However, T cells isolated from mice xenografted with KO PC and GB cells showed levels of proliferation and IL-2 expression similar to those measured in T cells from control mice (Fig. 7 *A* and *B*). Furthermore, flow cytometry analysis of those cells revealed that, compared to T cells from control mice, T cells from mice grafted with WT PC and GB presented significant higher levels of 2 coinhibitor receptors associated with suppression of T cell function in the tumor microenvironment: PD-1 and cytotoxic T lymphocyte-associated protein-4 (CTLA-4). However, T cells isolated from mice grafted with KO PC and GB showed no significant increase in the expression of those receptors (Fig. 7*C* and *SI Appendix*, Fig. S6*A*). Corroborating those data, we also found high PD-1 expression in T cells infiltrating the meninges of mice that were grafted with WT PC and GB, whereas mice that received KO PC and GB did not show any infiltration in the meninges (Fig. 7*D*). In the perivascular areas, where PC make contacts with GB cells, approximately the same levels of T cell infiltration (40 to 60%) were detected in mice with WT PC and GB and in mice that received KO PC and GB. However, almost all T cells expressed PD-1 in mice that received WT PC, but just 1 to 2% of T cells expressed PD-1 in mice with KO PC (*SI Appendix*, Fig. S6*B*).

Supporting previous data, we also found increased expression of the T regulatory cells transcription factor FoxP3 in isolated T cells from cervical and maxillary lymph nodes and in T cells infiltrating the perivascular areas close to meningeal and tumor areas (~25% of the total) of mice that were grafted with WT PC and GB (*SI Appendix*, Fig. S7 *A–C*). Mice that were xenografted with KO PC and GB showed increased levels of antigen-specific central memory ($CD44^+$ $CD62^+$) $CD4^+$ and $CD8^+$ T cells compared to those xenografted with WT PC and GB (*SI Appendix*, Fig. S7 *D–G*). Many T cells in the infiltrates showed an effector/memory $CD44^+$ phenotype, and were surrounding perivascular areas near the tumor area (ratio $CD4^+$:$CD8^+$ = 4:1). Mice that were xenografted with KO PC and GB, presented higher levels of $CD44^+$ cells and increased infiltration of $CD8^+CD44^+$ T cells (ratio $CD4^+$:$CD8^+$ = 2:1) in those areas of the brain parenchyma where there were barely any remaining GB cells (*SI Appendix*, Fig. S7 *A* and *H*).

Downloaded at Palestinian Territory, occupied on December 9, 2021
www.manaraa.com

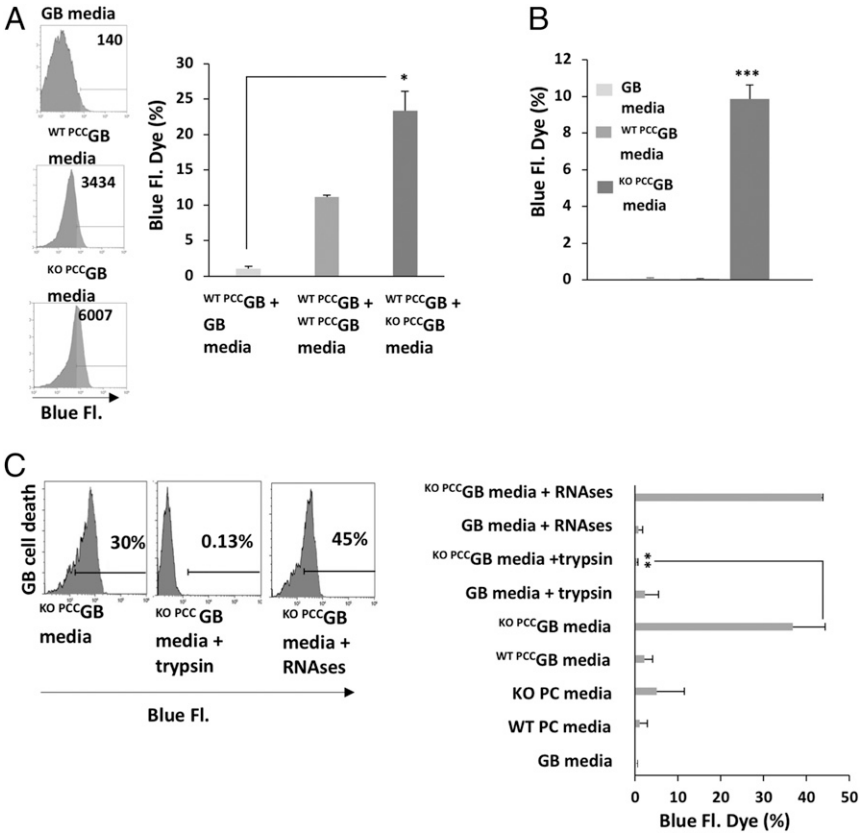

Fig. 5. GB-induced CMA in PC prevents an anti-tumor protein secretion to maintain GB cell survival. (*A*) Flow cytometry analysis, using LIVE/DEAD blue-fluorescent dye, GB cell death when cultured with WT PC in presence or not of conditioned media from 72-h cocultures of GB and WT PC or GB and KO PC (PC death cell was not detectable). MFI is shown in representative histograms and graph bar represents quantification of dead cell percentages from at least 3 independent experiments; $*P < 0.05$. (*B*) Flow cytometry analysis of the percentage of GB cell death. GB cells were cultured in presence of media obtained from cocultures of GB and WT PC or GB and-KO cultured for 72 h and compared to cells grown in control GB cell media. Data are mean ± SD of 3 independent experiments; $***P < 0.001$. (*C*) Detection of GB cell death by blue-fluorescent dye, following cocultured with WT PC in presence of conditioned media from 72-h cocultures of GB and KO PC pretreated with trypsin or RNase. Histograms are representative experiments of the quantification shown in the bar graph. Data are mean ± SD of 3 independent experiments. Values are also shown for pretreated control media and media from control GB cells, WT PC, or KO PC; $**P < 0.01$.

Interestingly, those areas also showed high expression of CD44, possibly indicating glial activation (40) (*SI Appendix*, Fig. S7*H*).

We had seen previously that xenografted mice with WT PC and GB show higher tumor growth than mice grafted with only GB (4). Interestingly, we found only residual numbers of RFP^+ GB cells in the infiltrated areas of mice grafted with KO PC and GB (Fig. 7 *E*, *Left*). Those cells were also negative for the proliferation marker K_i67 (Fig. 7 *E*, *Right*). To confirm our in vitro data, we analyzed the expression of LAMP-2A in GB tumor areas and compared it to peritumoral areas in contact with blood vessels, where PC are located and GB infiltrates. Xenografted mice with GFP^+ WT PC and GB cells showed stronger expression of LAMP-2A next to perivascular areas than inside or outside the tumor area (Fig. 7*F*). Those tumor infiltration areas expressing higher LAMP-2A levels accumulated GFP^+ PC. Confirming previous results, part of the strong LAMP-2A expression colocalized with GFP^+ PC, suggesting that GB-interacting GFP^+ PC may have higher CMA activity than other areas inside or outside the tumor where endogenous PC may be located (Fig. 7*F* and *SI Appendix*, Fig. S6*C*). Finally, supporting that CMA activity was also induced in human tumors, we found increased LAMP-2A expression around blood vessels of brain human biopsies from GB patients, where PC are situated and GB infiltrates (Fig. 7*G*). PC were identified by the NG2 PC marker colocalizing with LAMP-2A expression (*SI Appendix*, Fig. S6*D*).

Discussion

Several mechanisms have been reported to facilitate GB progression (6–10), including the formation of a functional network that may require cell interactions for cell intercommunication and delivery of molecules that assist tumor survival (3, 4, 11). Tumor cell infiltration and invasion in the brain parenchyma occurs through white matter tracts, subpial spread, perineural region, and also through perivascular areas where PC are situated, leading to direct cell interactions between GB cells and PC (4, 5, 11–14). These interactions, instead of promoting the PC inflammatory function (16–19), make them acquire an immunosuppressive function that assists in the establishment of immune tolerance and, therefore, facilitates tumor growth (4). However, the mechanisms that regulate GB tumor cell–PC interactions and the induction of an immunosuppressive phenotype in those PC are currently unknown.

In this work, we report that GB induces CMA activity in PC, and that this aberrant increase in CMA activity is the mechanism responsible for 1) switching PC immune function and 2) promoting more stable interactions with GB, which help maintaining tumor survival and prevent secretion of proteins with antitumor activity (Fig. 6*G*).

Our data show that the interaction of GB with PC induces up-regulation of LAMP-2A protein levels, the lysosomal membrane receptor for CMA, which leads to increased CMA activity. This occurs preferentially in peritumoral areas, where GB cells are actively interacting with the perivascular space where PC are located (Fig. 7 *F* and *G* and *SI Appendix*, Fig. S6*C*). GB-mediated up-regulation of LAMP-2A protein levels in PC occurs as a consequence of a burst in ROS generation that follows GB–PC interaction (Fig. 1). Our results indicate that production of high levels of ROS starts shortly after interaction between PC and GB occurs. Changes in ROS levels are hardly detected in nonhypoxic PC (*SI Appendix*, Fig. S1*A*) but are rapidly produced by GB upon interaction with PC (Fig. 1*G*). Confirming that the ROS burst is necessary to up-regulate LAMP-2A protein levels in PC, we found that this up-regulation was prevented in the presence of a ROS scavenger (Fig. 1*H*). Furthermore, using a luciferase reporter containing the promoter of the *Lamp2* gene bearing ROS responsive elements (25, 26), we confirmed that *Lamp2a* was induced in PC in response to ROS in PC grown in conditioned media from GB–PC cocultures (*SI Appendix*, Fig. S1*A*). Induction of *Lamp2a* expression mediated by increased generation of ROS has been previously described in fibroblasts exposed to oxidative stress (26). Our results support that GB may hijack this mechanism, which cells use to activate CMA and cope with oxidative stress, to instead induce changes in PC that eventually facilitate tumor survival and progression.

Downloaded at Palestinian Territory, occupied on December 9, 2021
www.manaraa.com

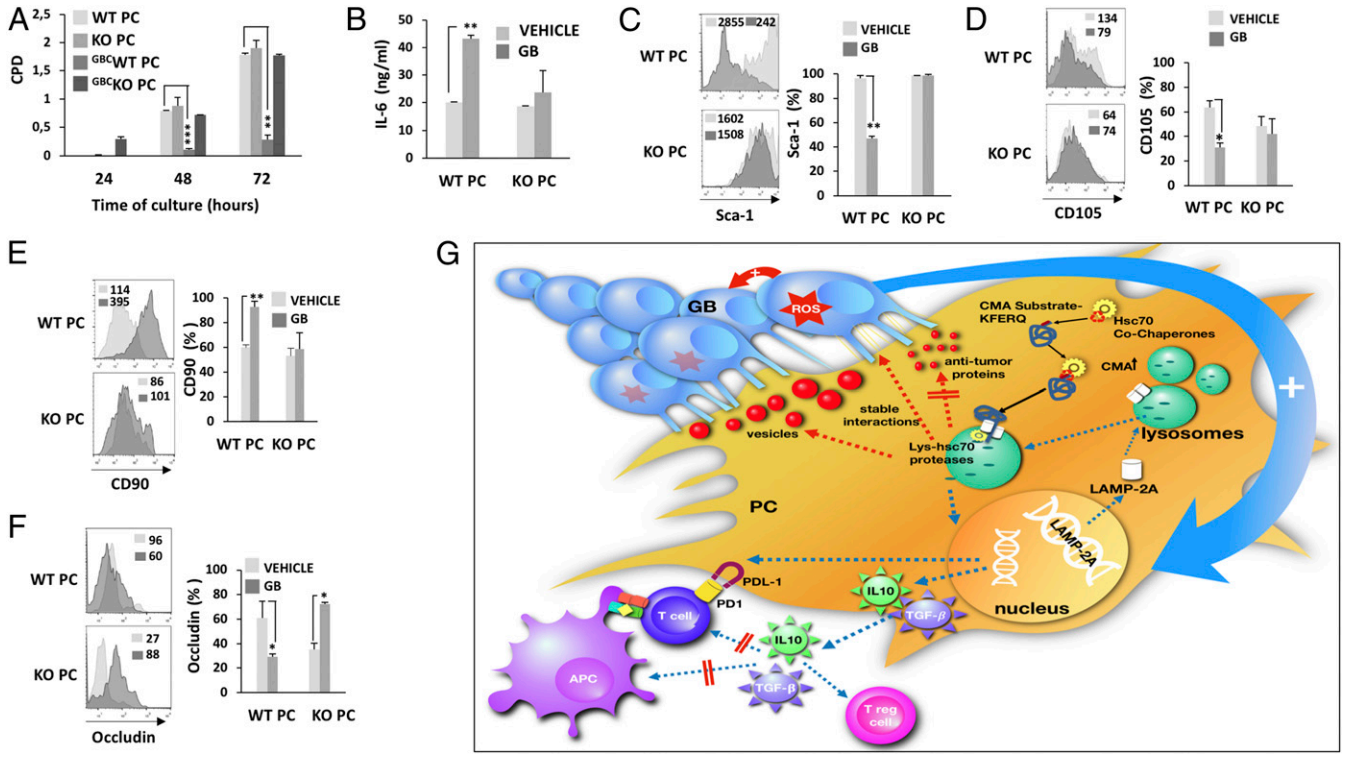

Fig. 6. GB-induced CMA in PC alters the expression of markers/properties associated with MSC and contributes to regulate interactions with GB cells. (*A*) Proliferation of WT PC and KO PC interacting with GB cells measured as CPD at different times of coculture compared to proliferation of control PC. Results are mean + SD of at least 3 different experiments; $^{**}P < 0.01$, $^{***}P < 0.001$. (*B*) Mouse IL-6 production was measured by ELISA in WT and KO PC cultured for 72 h with GB cells. All data represent mean ± SD obtained from at least 3 independent experiments; $^{**}P < 0.01$. (*C–F*) Flow cytometry analysis of the expression of Sca-1, CD105, and CD90 in WT PC (*Upper* histograms) and KO PC (*Lower* histograms) conditioned or not by GB cells for 72 h. Gate strategy to separate both cell populations was performed as indicated in Fig. 1*E*. Insert numbers inside histograms represent MFI values for representative plots. Bar graphs represent percentages of positive cells expressing every marker. Nonspecific fluorescence was measured using isotype monoclonal antibodies and GB cells were used as negative controls. Data represent mean ± SD obtained from at least 3 independent experiments; $^{*}P < 0.05$; $^{**}P < 0.01$. (*F*) Flow cytometry analysis of the expression of occludin in WT PC (*Upper* histograms) and KO PC (*Lower* histograms) conditioned or not by GB cells for 48 h. Insert numbers inside histograms represent MFI values for representative results. Bar graph represent percentages of positive cells. Nonspecific fluorescence was measured using isotype monoclonal antibodies and GB cells were used as negative control. Data represent mean ± SD obtained from at least 3 independent experiments; $^{*}P < 0.05$. (*G*) Proposed model depicting how GB induced CMA affects the PC functions. GB-induced CMA promotes an immunosuppressive function in PC that fails to support T cell responses GB (blue arrows). GB interaction with PC promotes a ROS burst that leads to increased up-regulation of the LAMP-2A expression in PC (big blue arrow). LAMP2-A is delivered to the lysosomal membrane to increase CMA activity (blue dashed arrows) (21, 31). The Hsc70 chaperone recognizes KFERQ motifs in CMA substrate proteins and with the help of its cochaperones, delivers them to the lysosomal membrane where they interact with LAMP-2A and are translocated, not the lysosomal lumen assisted by a resident luminal Hsc70. Modulation of the PC proteome eventually results in changes in programs of gene expression that include up-regulation of the antiinflammatory cytokines TGF-β and IL-10, which exert a negative regulation on T cells and antigen presenting cells (blue arrows). T cell activation and proliferation are affected and regulatory T cells are generated. The absence of costimulatory molecules, such as CD80 and CD86, and the expression of the negative regulator PDL-1, also facilitate an immunosuppressive function in PC. Degradation of specific substrate proteins may also regulate distinct functions in PC that are lost or gained as a consequence of the induction of CMA by GB. GB-induced CMA in PC also modulates their MSC-like properties and stabilizes GB–PC interaction to facilitate tumor growth (big red arrow). Specifically, inhibition of the secretion of proteins that may have antitumor activity and an increase in the secretion of vesicles with proregenerative factors, may also assist tumor proliferation (red dashed arrows).

Our data corroborate previous studies from our group that showed the ability of GB to prevent antitumor inflammatory responses in PC (4) and identify GB-induced CMA as a contributing mechanism to that effect (Fig. 2). Indeed, when GB interacts with CMA-deficient PC, these cells fail to acquire the antiinflammatory phenotype and the immunosuppressive function usually seen in ^{GBC}WT PC. Instead, PC become proinflammatory and able to induce effective T cell responses (Fig. 2). Abnormal up-regulation of CMA in PC could be an efficient way to degrade or interfere with the generation and release of the cytotoxic products that should contribute to the immune response of PC against the tumor. By doing so, the activation of CMA in ^{GBC}PC would permit instead the establishment of a GB-induced immunosuppressive function in PC.

GB-induced CMA in PC is also required to maintain effective interactions between GB cells and PC, which is crucial for tumor cell survival and proliferation (Fig. 3). GB is able to recruit and modify the function of different cell types in the brain, including PC, to generate a microenvironment that favors tumor growth and prevents an antitumor immune response. This is achieved not only through the secretion of soluble mediators but also through cell-to-cell direct communication mediated by nanotubes and extracellular secretory vesicles that can transport proteins, metabolites, macromolecules, or even whole organelles between cells (3, 41). We have found that, whereas GB established an organized network of nanotube-mediated connections with WT PC, it failed to do so in the presence of CMA-deficient KO PC. Furthermore, the accumulation of vesicles that was observed in the contact site between PC and GB were almost absent in the presence of LAMP-2A–deficient PC. These data suggest that CMA activity induced by GB in PC might contribute to the turnover of proteins involved in the regulation of the formation and maintenance of those nanotubes, and down-regulate the generation and secretion of extracellular vesicles that normally carry cytotoxic products able to kill tumor cells. We propose that this cytotoxicity resulted directly from the

Downloaded at Palestinian Territory, occupied on December 9, 2021
www.manaraa.com

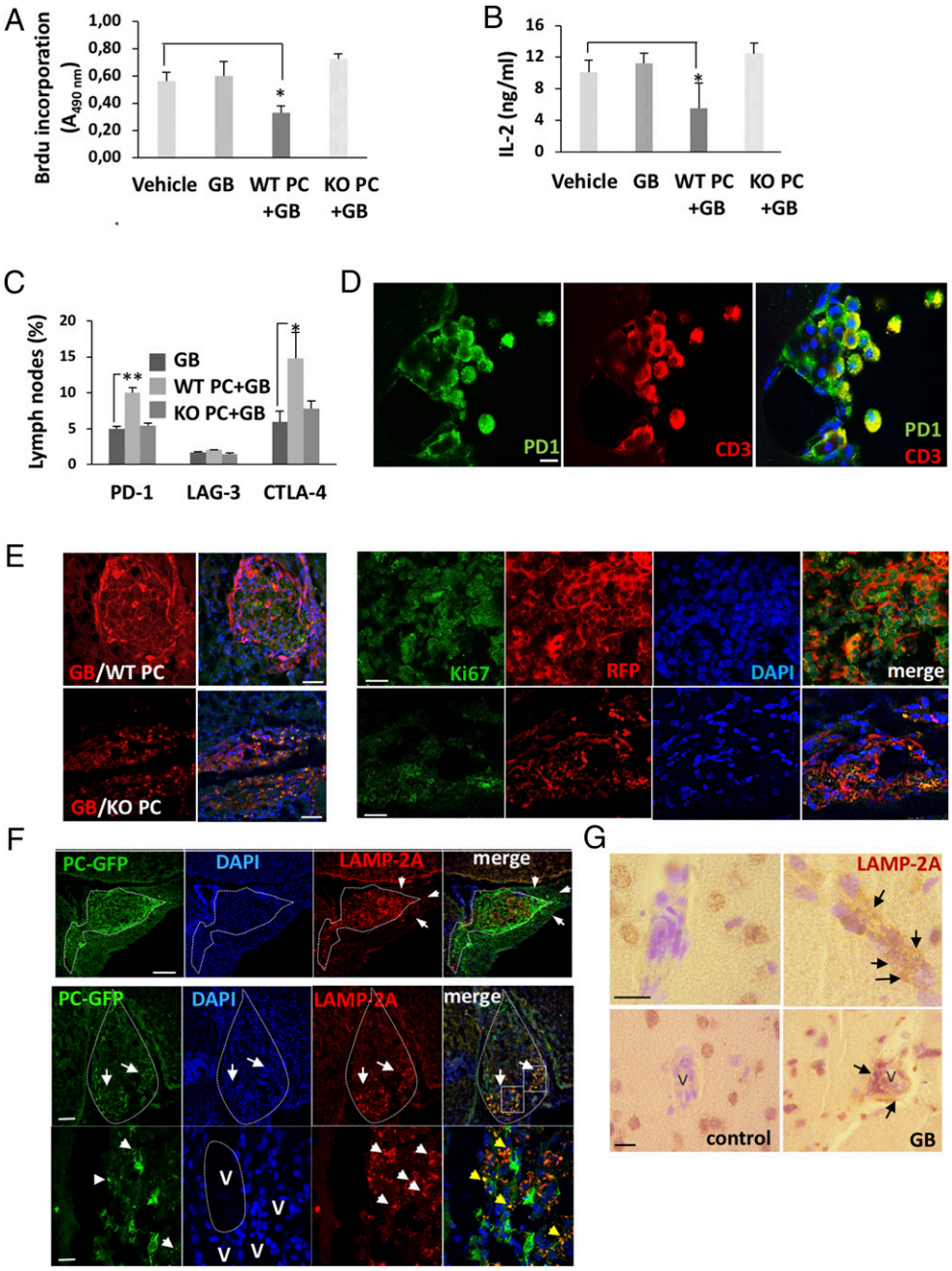

Fig. 7. GB-induced CMA in PC assists tumor growth. (*A*) Activation-induced cell proliferation and (*B*) IL-2 production were measured in $CD4^+$ T cells isolated from maxillary and cervical lymph nodes from xenografted mice with WT PC and GB cells (WT PC+GB) or KO PC and GB cells (KO PC+GB) and compared to T cells from control mice xenografted with GB cells or PBS (vehicle). Cells were activated ex vivo with anti-CD3 and anti-CD28 for 72 h. All data represents mean ± SD of at least 3 independent experiments; $*P < 0.05$. (*C*) Flow cytometry analysis of the expression if coinhibitory receptors in $CD4^+$ T cells isolated from lymph nodes (maxillary, cervical, and axillary) from xenografted mice with WT PC and GB cells (WT PC+GB) or KO PC and GB cells (KO PC+GB) and compared to T cells isolated from control mice xenografted with GB cells. $*P < 0.05$; $**P < 0.01$. (*D*) Expression of PD-1 was detected by immunofluorescence in T cells from the cerebrospinal fluid of meninges of grafted mice with GB and WT PC. (Scale bar, 10 μm.) (*E*) GB tumor growth in mice that were xenografted with cocultures of WT PC+GB cells (GB/WT PC) and compared to mice xenografted with KO PC+GB cells (GB/KO PC) (Scale bars of *Left*, 250 μm.) *Right* shows representative detail of proliferating GB cells, which appear as intense RFP^+ fluorescent spherical dividing cells (red) and K_i67^+ (green). Confocal microphotographs (1-μm-thick section). (Scale bar, 50 μm.) (*F*) Expression of LAMP-2A in PC and GB cells in xenografts of cocultured PC expressing GFP (PC-GFP) and GB cells. *Upper* shows delimited tumor with heterogenous and stronger expression of LAMP-2A in the right pole next to perivascular areas (arrows). Merged image of confocal microphotographs (1-μm-thick section) shows the colocalization of LAMP-2A expression in the GB cells and perivascular cells. (Scale bar, 100 μm.) *Lower* shows PC in those tumor infiltration areas as GFP^+ cells (green). These cells accumulated in the ventral pole of the tumor (arrows). (Scale bar, 250 μm.) Nuclear staining by DAPI (blue) shows that tumor cellularity was higher in the ventral pole (arrows). Strong LAMP-2A (red) expression in the ventral pole of the tumor is indicated (arrows) and compared to the rest of the tumor where hardly any GFP^+ PC are localized. Merged image shows the colocalization of grafted PC and the strong expression of LAMP-2A in the peritumoral areas and around blood vessels, where also endogenous PC of the mice are situated. *Insets* show the areas in detail of bottom pictures. High power pictures showing GFP^+ and $LAMP\text{-}2A^+$ punctate pattern (arrowheads) colocalization around blood vessels (V). (Scale bar, 45 μm.) All Images are representative of data from GB+WT PC grafted mice (12 tumors/15 grafted mice) and GB+KO PC grafted mice (0 tumors/15 grafted mice). Mice were analyzed 4 to 11 wk after graft. Images are representative of at least 3 different experiments using U87 or U373 GB lines independently. (*G*) Representative images of LAMP-2A expression (arrows) in perivascular areas (V) of 8 brain biopsies from GB patients compared to 6 control fields in the not infiltrated brain areas. (Scale bar, 50 μm.)

Downloaded at Palestinian Territory, occupied on December 9, 2021
www.manaraa.com

secreted components rather than from the inability to sustain the tumor–PC interactions, because conditioned media from GB–KO PC cocultures were able to kill GB cells even if they were interacting with WT PC (Figs. 4 and 5).

Constitutive high levels of GM-CSF produced by GB have been reported to promote immunosuppression of the antitumor immune response (8, 42). Corroborating previously reported data, we found production of higher levels of GM-CSF in GB following interaction with WT PC compared to basal levels. Interestingly, CMA-deficient PC also promoted significant changes in GB that translated in production of even higher GM-CSF and ROS levels (Fig. 4), which could be reproduced by culturing GB in conditioned media from cultures of GB with KO PC (Fig. 4 *B* and *E*). This increased production of GM-CSF and ROS correlated with GB cell death (Fig. 5). These data suggest that the dual role of GM-CSF as stimulatory or suppressive of the immune response depends in part on the dose (8, 42), and on the establishment of GB interactions with cells of the brain parenchyma.

Our data show that GB-induced CMA activity in PC regulates markers/properties associated with MSC in those PC, including proliferation, expression of MSC markers, production of cytokines, and proregenerative factors (Fig. 6 and *SI Appendix*, Fig. S4), as well as their immune function. Up-regulation of the expression of occludin in PC, which is dependent on GB-induced CMA (Fig. 6*F* and *SI Appendix*, Fig. S5*B*), might also contribute to the stabilization of GB–PC interactions (34). This may account for the unstable interactions observed between GB and CMA-deficient PC. We found that all changes detected on PC were dependent on GB-induced CMA, which suggests that GB may promote the abnormal up-regulation of this selective form of autophagy in PC to subvert PC's antitumor responses through the degradation of proteins that may participate in the expression of inflammatory mediators, the regulation of MSC-like properties, or the maintenance of effective cell-to-cell communication. An in-depth study of changes in the proteome of WT or LAMP-2A–deficient PC in the presence of GB will be required to identify CMA substrates that may be involved in modulating all these changes.

In vitro and in vivo data also supports that GB-induced CMA in PC is essential for PC to acquire an immunosuppressive function (Fig. 6*G*), which prevents effective antitumor T cell responses. Consequently, only when GB and WT PC were grafted, T cells from tumor-bearing mice expressed higher levels of inhibitory receptors (Figs. 2 and 7 *A–D*), and showed decreased responses to activation, which eventually resulted in increased tumor cell survival and proliferation (Figs. 3, 6*G*, and 7*E*), and facilitated tumor progression (Fig. 7*E*) (4). Those changes were not present when GB was grafted with KO PC, which may account, at least in part, for the hindered tumor progression observed in those animals.

Multiple immune cell populations—including myeloid-derived suppressor cells, microglia, and astrocytes—might participate in the suppression of the immune response in the tumor microenvironment. This may occur through the regulation of several mechanisms that may be responsible for GB immune evasion (43, 44). Our work highlights PC as a cell type that is essential for the establishment of immune evasion in GB. Modulation of CMA activity, however, can revert the immunosuppressive phenotype that PC acquire in the presence of GB and contribute to the generation of an effective antitumor immune response.

In recent years, several preclinical and clinical studies have demonstrated that interventions using immune checkpoint inhibition as a single therapy, including blockade of PD-1/PD-L1 or CTLA-4/B7-1/B7-2 interactions, can be effective for several types of cancer, including melanoma or lung cancer, but fail to induce effective antitumor responses in others, such as GB (45, 46). The lack of the generation of highly immunogenic antigens during GB progression and the subsequent failure in the T cell response seems to facilitate GB escape from the immune system, together with the establishment of an immunosuppressive microenvironment using mechanisms that may be resistant to checkpoint inhibition (45, 46). Our results support that the induction of CMA in PC caused by GB participates in the regulation not only of the expression of coinhibitory receptors, such as PD-1 and CTLA-4, but also of other mechanisms responsible for GB-induced immunosuppression. Excitingly, when CMA activation is prevented in PC, increased numbers of memory T cells are detected, which correlates with efficient GB growth control. Those T cells may represent cells that have been activated by tumor antigens and might be able to generate an efficient antitumor response (Fig. 7 and *SI Appendix*, Figs. S6 and S7).

Our work shows that GB-induced CMA in PC may provide a critical element for the local control of PC–tumor cell interaction and for the down-regulation of the antitumor immune response. Therefore, preventing the GB-induced up-regulation of CMA in the contacting PC may represent a targeting strategy for the development of new therapies against GB.

Materials and Methods

Mice. Six- to 8-wk-old WT C57BL/6, C57BL/6-Tg (ACTB-EGFP)1Osb/J (Charles River Laboratory), Tg(TcraTcrb)425Cbn/j (OT-II) TCR transgenic (Jackson Laboratory) mice were maintained in pathogen-free conditions in the animal facilities of the University of Murcia and Biomedical Research Institute of Murcia-Arrixaca. All animal procedures were approved and performed according to the guidelines set by the University of Murcia Institutional Animal Care and Use Committee.

Cell Culture. Primary brain PC from mice were isolated and cocultured with GB cells, at a ratio 1:1 for 12 to 72 h, as described previously (4). PC with impaired CMA, were isolated from brains of *Lamp2a*$^{-/-}$ mice (47). Alternatively, *Lamp2a* expression was silenced by transducing PC with lentivirus expressing *Lamp2*-specific shRNAs as described in *SI Appendix*. Human GB cell lines U373-MG and U87 were purchased from European Collection for Authenticated Cell Cultures. Cell culture media obtained from 72-h cocultures of GB and PC was concentrated using Amicon Ultra centrifugal filters 10k (Millipore) and used 10 times diluted. PC were pretreated with a ROS scavenger, NAc (Sigma) at 20 mM and after cocultured with GB for 48 h at 500 μM. DiD labeling solution (Invitrogen), GFP-expressing PC, and GB expressing RFP were used for cell tracking, cell population separation, and sorting (Sony SH800) as described previously (4). For the vesicular fraction isolation, quantification, and function in PC, please see *SI Appendix*.

Primary CD4$^+$ T cells were isolated from lymph nodes using anti-CD4–coupled magnetic beads (Life Technologies). Isolated T cells were stimulated ex vivo with 0.5 μg/mL plate bound anti-CD3 and 0.5 μg/mL anti-CD28 (BD Biosciences). Functional assays of PC with T cells were carried out as described previously (4).

Real-Time PCR (qPCR). cDNA was synthesized from total mRNA, and gene expression was analyzed by real-time PCR using SYBR Green in a Step One Plus Thermocycler (Applied Biosystems), as described previously (4). For primer sequence information, please see *SI Appendix*.

Immunoblotting. Total cellular lysates were prepared using RIPA buffer (1% Triton-X 100, 1% sodium deoxycholate, 0.1% SDS, 0.15 M NaCl, 0.01 M sodium phosphate, pH 7.2). Primary antibodies used were rabbit anti-mouse LAMP-2A (Invitrogen), rabbit anti-mouse GFP (Abcam), and anti–β-actin (Santa Cruz Biotechnology). For plasmid transfection, reporter assays, and lentiviral infection, please see *SI Appendix*.

ELISA. PC (5×10^4) were cultured with GB cells at 1:1 ratio in 96-well plates for 24 to 72 h. Mouse TNF-α, IL-6, VEGF (R&D Systems), angiotensin (Abcam), antithrombin, and osteonectin (Abyntek) secreted by PC in the media or in vesicles (for vesicles preparation, quantification and function, please see *SI Appendix*) and GM-CSF (Diaclone) secretion by GB, as well as IL-2 (BD Biosciences) production by T cells were measured by sandwich ELISA with specific antimouse antibodies following the manufacturer's recommendations.

Flow Cytometry Analysis. Lysotracker and mitotracker were used for lysosomes and mitochondria tracking (Invitrogen). ROS production was measured using the H2DCFDA probe (Invitrogen). Expression of CD80, CD90 (eBioscience), Sca-1 (Biolegend), CD105 (Abcam), occludin (ProSci Inc; Thermofisher), PD-1 (Novus), CTLA-4, LAG-3, CD4, CD3, FoxP3 (eBioscience), CD44 (BD Biosciences), and CD62L (Palex) were analyzed using DiD labeling solution for tracking and separation of cells and specific anti-mouse antibodies. Labeled isotype monoclonal antibodies were used on GB to determine background nonspecific fluorescence. PC and GB cell death was determined using LIVE/DEAD Fixable

Downloaded at Palestinian Territory, occupied on December 9, 2021
www.manaraa.com

Blue Dead Cell Stain Kit, (ThermoFisher). Stained cells were analyzed by flow cytometry using a FACSCanto flow cytometer (BD Bioscience) and data were analyzed with Kaluza analysis software (Beckman Coulter).

Adhesion Assay. GB cells expressing RFP and previously irradiated to inhibit their proliferation and just analyze cell adhesion, were cocultured on a monolayer culture of WT PC or KO PC for 24 h. Cells were lysed after washing away non-adhered cells with media and remaining RFP fluorescence in the wells (belonging to the GB that adhered to PC) was measured at 488 nm (588-nm emission). Purified cell media from cocultures of GB and *Lamp2a*$^{-/-}$ PC was treated with RNase (Qiagen) or trypsin (Sigma) and added to PC, before or after 48 h of cocultured with GB.

Proliferation Assay. PC (5×10^4) were cultured with GB cells at 1:1 ratio in 6-well plates for 24 to 72 h. Isolation, counting and cumulative population doubling level were measured as previously described (4). In some cases, 5-(and 6)-Carboxyfluorescein diacetate succinimidyl ester (CFSE) was also used as cell proliferation tracker (eBioscience). T cell proliferation was measured by BrdU incorporation using a commercial kit (Roche), as previously described (4).

Xenografts. Cell pellets from human GB cells or GB cells cocultured with murine PC for 72 h (5×10^6 cells), were grafted into C57BL/6 mice brains. Xenografts were performed as described previously in an immunocompetent mouse model (4). Fifteen mice received xenografts and were analyzed in each experimental line (GB, GB+WT PC and GB+KO PC). Eleven weeks postgrafting, mice were perfused using 4% paraformaldehyde (Panreac). Brains were embedded in 30% sucrose (Sigma) and cut at 4-μm using a cryostat. For immunohistochemistry in xenografts and GB patient samples, immunofluorescence, and scanning electron microscopy, please see detailed *SI Appendix, Supplementary Materials and Methods*.

Statistical Analysis. Differences between groups were analyzed by 1-way ANOVA with a Tukey–Kramer posttest. Comparisons between data pairs were analyzed using a *t* test. Statistical significance was defined as $P < 0.05$.

ACKNOWLEDGMENTS. We thank Dr. Pablo Pelegrín's laboratory at the Experimental Surgery Unit, Biomedical Research Institute of Murcia-Arrixaca, for his always kind help providing tools for this study; Prof. Pedro Aparicio at the Immunology Department of University of Murcia for all his kind and helpful discussions about this study; and the Anatomy Department of the College of Medicine, the Microscopy and Cell Culture facilities at the University of Murcia, and the Animal facility of Biomedical Research Institute of Murcia-Arrixaca, for their technical support. This work was funded mainly by Ministerio de Economía y Competitividad de España (MINECO) SAF2015-73923-JIN and Fondo Europeo de Desarrollo Regional/Union Europea (AEI/FEDER/UE) (to R.V.). It was supported partially by Mobility Seneca Foundation Grant "Programa Jimenez de la Espada, 19667/EE/14 (to R.V.); Seneca 20840/PI/18 (to R.V.); ISCIII/Red de Terapia Celular, TERCEL RD16/0011/0010 and RD16/0011/0001 (to S.M. and J.M.M.); and NIH P01 AG031782 (to F.M. and A.M.C.).

1. D. Hambardzumyan, G. Bergers, Glioblastoma: Defining tumor niches. *Trends Cancer* **1**, 252–265 (2015).
2. P. Y. Wen, D. A. Reardon, Neuro-oncology in 2015: Progress in glioma diagnosis, classification and treatment. *Nat. Rev. Neurol.* **12**, 69–70 (2016).
3. M. Osswald *et al*., Brain tumour cells interconnect to a functional and resistant network. *Nature* **528**, 93–98 (2015).
4. R. Valdor *et al*., Glioblastoma progression is assisted by induction of immunosuppressive function of pericytes through interaction with tumor cells. *Oncotarget* **8**, 68614–68626 (2017).
5. A. Farin *et al*., Transplanted glioma cells migrate and proliferate on host brain vasculature: A dynamic analysis. *Glia* **53**, 799–808 (2006).
6. E. K. Nduom, M. Weller, A. B. Heimberger, Immunosuppressive mechanisms in glioblastoma. *Neuro. Oncol.* **17** (suppl. 7), vii9–vii14 (2015).
7. M. Preusser, M. Lim, D. A. Hafler, D. A. Reardon, J. H. Sampson, Prospects of immune checkpoint modulators in the treatment of glioblastoma. *Nat. Rev. Neurol.* **11**, 504–514 (2015).
8. R. E. Kast *et al*., Glioblastoma-synthesized G-CSF and GM-CSF contribute to growth and immunosuppression: Potential therapeutic benefit from dapsone, fenofibrate, and ribavirin. *Tumour Biol.* **39**, 1010428317699797 (2017).
9. L. Cheng *et al*., Glioblastoma stem cells generate vascular pericytes to support vessel function and tumor growth. *Cell* **153**, 139–152 (2013).
10. W. Zhou *et al*., Periostin secreted by glioblastoma stem cells recruits M2 tumour-associated macrophages and promotes malignant growth. *Nat. Cell Biol.* **17**, 170–182 (2015).
11. A. B. Hjelmeland, J. D. Lathia, S. Sathornsumetee, J. N. Rich, Twisted tango: Brain tumor neurovascular interactions. *Nat. Neurosci.* **14**, 1375–1381 (2011).
12. P. Carmeliet, R. K. Jain, Molecular mechanisms and clinical applications of angiogenesis. *Nature* **473**, 298–307 (2011).
13. C. M. Peppiatt, C. Howarth, P. Mobbs, D. Attwell, Bidirectional control of CNS capillary diameter by pericytes. *Nature* **443**, 700–704 (2006).
14. J. Cheng *et al*., Targeting pericytes for therapeutic approaches to neurological disorders. *Acta Neuropathol.* **136**, 507–523 (2018).
15. R. D. Bell *et al*., Pericytes control key neurovascular functions and neuronal phenotype in the adult brain and during brain aging. *Neuron* **68**, 409–427 (2010).
16. E. A. Winkler, R. D. Bell, B. V. Zlokovic, Central nervous system pericytes in health and disease. *Nat. Neurosci.* **14**, 1398–1405 (2011).
17. R. Daneman, L. Zhou, A. A. Kebede, B. A. Barres, Pericytes are required for blood-brain barrier integrity during embryogenesis. *Nature* **468**, 562–566 (2010).
18. A. Gaceb, M. Barbariga, I. Özen, G. Paul, The pericyte secretome: Potential impact on regeneration. *Biochimie* **155**, 16–25 (2018).
19. J. Rustenhoven, D. Jansson, L. C. Smyth, M. Dragunow, Brain pericytes as mediators of neuroinflammation. *Trends Pharmacol. Sci.* **38**, 291–304 (2017).
20. A. Gaceb, I. Özen, T. Padel, M. Barbariga, G. Paul, Pericytes secrete pro-regenerative molecules in response to platelet-derived growth factor-BB. *J. Cereb. Blood Flow Metab.* **38**, 45–57 (2018).
21. J. F. Dice, Peptide sequences that target cytosolic proteins for lysosomal proteolysis. *Trends Biochem. Sci.* **15**, 305–309 (1990).
22. S. Kaushik, A. M. Cuervo, The coming of age of chaperone-mediated autophagy. *Nat. Rev. Mol. Cell Biol.* **19**, 365–381 (2018).
23. H. L. Chiang, S. R. Terlecky, C. P. Plant, J. F. Dice, A role for a 70-kilodalton heat shock protein in lysosomal degradation of intracellular proteins. *Science* **246**, 382–385 (1989).
24. U. Bandyopadhyay, S. Kaushik, L. Varticovski, A. M. Cuervo, The chaperone-mediated autophagy receptor organizes in dynamic protein complexes at the lysosomal membrane. *Mol. Cell. Biol.* **28**, 5747–5763 (2008).
25. A. M. Cuervo, J. F. Dice, A receptor for the selective uptake and degradation of proteins by lysosomes. *Science* **273**, 501–503 (1996).
26. R. Valdor *et al*., Chaperone-mediated autophagy regulates T cell responses through targeted degradation of negative regulators of T cell activation. *Nat. Immunol.* **15**, 1046–1054 (2014).
27. R. Kiffin, C. Christian, E. Knecht, A. M. Cuervo, Activation of chaperone-mediated autophagy during oxidative stress. *Mol. Biol. Cell* **15**, 4829–4840 (2004).
28. A. C. Massey, S. Kaushik, G. Sovak, R. Kiffin, A. M. Cuervo, Consequences of the selective blockage of chaperone-mediated autophagy. *Proc. Natl. Acad. Sci. U.S.A.* **103**, 5805–5810 (2006).
29. R. Valdor, F. Macian, Autophagy and the regulation of the immune response. *Pharmacol. Res.* **66**, 475–483 (2012).
30. J. Chen *et al*., CD146 coordinates brain endothelial cell-pericyte communication for blood-brain barrier development. *Proc. Natl. Acad. Sci. U.S.A.* **114**, E7622–E7631 (2017).
31. K. Hosaka *et al*., Pericyte-fibroblast transition promotes tumor growth and metastasis. *Proc. Natl. Acad. Sci. U.S.A.* **113**, E5618–E5627 (2016).
32. S. Kaushik, A. M. Cuervo, Proteostasis and aging. *Nat. Med.* **21**, 1406–1415 (2015).
33. H. Koga, M. Martinez-Vicente, F. Macian, V. V. Verkhusha, A. M. Cuervo, A photoconvertible fluorescent reporter to track chaperone-mediated autophagy. *Nat. Commun.* **2**, 386 (2011).
34. V. Castro *et al*., Occludin regulates glucose uptake and ATP production in pericytes by influencing AMP-activated protein kinase activity. *J. Cereb. Blood Flow Metab.* **38**, 317–332 (2018).
35. M. Kon *et al*., Chaperone-mediated autophagy is required for tumor growth. *Sci. Transl. Med.* **3**, 109ra117 (2011).
36. G. Luengo-Gil *et al*., Antithrombin controls tumor migration, invasion and angiogenesis by inhibition of enteropeptidase. *Sci. Rep.* **6**, 27544 (2016).
37. T. Isaka *et al*., Altered expression of antithrombotic molecules in human glioma vessels. *Acta Neuropathol.* **87**, 81–85 (1994).
38. L. B. Rivera, R. A. Brekken, SPARC promotes pericyte recruitment via inhibition of endoglin-dependent TGF-β1 activity. *J. Cell Biol.* **193**, 1305–1319 (2011).
39. A. Chlenski *et al*., SPARC expression is associated with impaired tumor growth, inhibited angiogenesis and changes in the extracellular matrix. *Int. J. Cancer* **118**, 310–316 (2006).
40. H. Haegel, C. Tölg, M. Hofmann, R. Ceredig, Activated mouse astrocytes and T cells express similar CD44 variants. Role of CD44 in astrocyte/T cell binding. *J. Cell Biol.* **122**, 1067–1077 (1993).
41. C. Quezada *et al*., Role of extracellular vesicles in glioma progression. *Mol. Aspects Med.* **60**, 38–51 (2018).
42. I. S. Hong, Stimulatory versus suppressive effects of GM-CSF on tumor progression in multiple cancer types. *Exp. Mol. Med.* **48**, e242 (2016).
43. B. Otvos *et al*., Cancer stem cell-secreted macrophage migration inhibitory factor stimulates myeloid derived suppressor cell function and facilitates glioblastoma immune evasion. *Stem Cells* **34**, 2026–2039 (2016).
44. D. Henrik Heiland *et al*., Tumor-associated reactive astrocytes aid the evolution of immunosuppressive environment in glioblastoma. *Nat. Commun.* **10**, 2541 (2019).
45. D. Saha, R. L. Martuza, S. D. Rabkin, Macrophage polarization contributes to glioblastoma eradication by combination immunovirotherapy and immune checkpoint blockade. *Cancer Cell* **32**, 253–267.e5 (2017).
46. V. A. Arrieta *et al*., The possibility of cancer immune editing in gliomas. A critical review. *Oncoimmunology* **7**, e1445458 (2018).
47. J. L. Schneider *et al*., Loss of hepatic chaperone-mediated autophagy accelerates proteostasis failure in aging. *Aging Cell* **14**, 249–264 (2015).

Downloaded at Palestinian Territory, occupied on December 9, 2021

www.manaraa.com